Robust Shape Reconstruction and Optimal Transportation

Pierre Alliez, Simon Giraudot, David Cohen-Steiner

Robust Shape Reconstruction and Optimal Transportation

Pierre Alliez
Simon Giraudot
David Cohen-Steiner

Abstract. We describe a framework for robust shape reconstruction from raw point sets, based on optimal transportation between measures, where the input point sets are seen as distribution of masses. In addition to robustness to defect-laden point sets, hampered with noise and outliers, our approach can reconstruct smooth closed shapes as well as piecewise smooth shapes with boundaries.

1. Introduction

Assuming a geometric data set made out of points or slices, the process of shape reconstruction amounts to recovering a surface or a solid that matches these samples. This problem is inherently ill-posed as infinitely-many shapes may fit the data. One must thus regularize the problem and add priors such as simplicity or smoothness of the inferred shape. In addition, the increasing variety of sensors for acquiring point sets corresponds to a range of defects inherent to each sensor and associated acquisition process. The point sets may differ in terms of sampling, noise and outliers. In addition, the level of noise may vary within the same point set, depending on the type of noise, acquisition condition and light-material interaction. Our quest for robustness includes the ability to deal with variable noise.

Related Work. In past years the *smooth, closed case* (i.e., shapes without sharp features nor boundaries) has received considerable attention. Computational geometric approaches to surface reconstruction, commonly based on Delaunay triangulations, generally provide theoretical guarantees under specific sampling models [4, 7]. The search for increased robustness to noise led to a wide variety of methods involving denoising, integral computations, variational formulations or scale-space processes. Robustness to outliers has been investigated through outlier removal [17], data clustering [16], robust norms such as the $l1$-sparse norm [2], spectral methods [13], or robust distances. However, state-of-the-art methods have several shortcomings: in addition to being generally not robust to outliers and not sufficiently robust to noise, they often require additional input attributes, such as lines of sight or oriented normal vectors [12].

Moving from the smooth, closed case to the *piecewise smooth case* (possibly with boundaries) is considerably harder as the ill-posedness of the problem applies to each sub-feature of the inferred shape. Further, very few approaches tackle the combined issue of robustness (to sampling defects, noise and outliers) and feature reconstruction [9, 1], and none to our knowledge addresses all the issues from heterogeneous data.

Positioning. In this work we develop shape reconstruction methods that are robust under perturbations of the data in the sense of the optimal transportation distance, the input point samples

Funded by ERC Starting Grant "IRON: Robust Geometry Processing", Grant agreement 257474.
Keywords: shape reconstruction, optimal transportation, noise robustness, outlier robustness.
Math. classification: 51XX.

being considered as Dirac measures. Optimal transportation refers to the problem of optimizing the cost of transportation of resources [18]. An intuitive example of optimal transport consists in determining the most effective way to move a pile of sand to a hole of the same volume. Most effective herein means that the integral of the distances the sand is moved, one infinitesimal unit of volume at a time, is minimal. This formulation of the problem, referred to as Monge's variational formulation, assumes that the sand is moved through a point-to-point mapping denoted by the transport plan. This restriction was relaxed by Kantorovich who extended the formulation to deal with transport plans between two probability measures. Optimal transportation reveals a versatile framework for geometry processing when observing that it can robustly measure distances between surfaces [14], and more generally between measures, be they discrete or continuous [5]. In addition to being symmetric, this distortion measure is by construction noise and outlier robust, a highly desirable feature when seeking robustness to defect-laden data. It has also been used for surface comparison [14] and displacement interpolation [3].

2. **Smooth Reconstruction**

We first focus on shapes that are both smooth and closed (with no boundary). We describe a recent noise-adaptive robust distance function which relies on the only assumption that the inferred shape is a smooth submanifold of known dimension [10]. Our algorithm takes as input a raw point set sampling the boundary of the inferred solid object.

Chazal et al. [5] introduced a robust distance function from a query point x to a measure μ in $\mathbb{R}$:

$$d^2_{\mu,m} : \mathbb{R}^n \to \mathbb{R},\ x \mapsto \frac{1}{m} \int_{B(x, r_{\mu,m}(x))} \|x - y\|^2 \mathrm{d}\mu(y),$$

where $m \in (0; 1]$ denotes a user-defined mass and $r_{\mu,m}$ denotes the minimal radius such that the ball $B(x, r_{\mu,m}(x))$ encloses this mass m. Considering the input point set as a distribution of n point masses, this simplifies to a sum on the K nearest neighbors.

In our quest for robustness, this function exhibits two relevant properties that are its robustness in the Wasserstein distance, and the 1-semiconcavity of its square. In addition, it is shown that under suitable sampling conditions, the sublevel sets of this distance function provide a homotopically correct approximation of the inferred shape, even in the presence of noise and outliers.

Mullen et al. [15] used these properties of the distance function to surface reconstruction with robustness to noise, outliers and missing data. A major limitation of this approach comes from the mass parameter K which must be user-specified: there is no principled way to select it automatically and it requires a trial-error process to trade robustness for accuracy. In addition, K is a global parameter and hence can not deal with non-uniform noise. The first two curves of Figure 3 show the behavior of the function on a point set with variable noise.

We now define a noise-adaptive distance function that solely relies on a dimension assumption: the inferred shape is a smooth submanifold of known dimension k embedded in a space of dimension d. For an input measure μ and a constant parameter $\alpha > 0$, we define the adaptive distance function as follows:

$$\delta_{\mu,\alpha} = \inf_{m>0} \frac{d_{\mu,m}}{m^\alpha}.$$

First, consider the case of an ambient noise μ in dimension d as shown on Figure 1 (left). The distance function simplifies to $d^2_{\mu,m} = c_1 m^{2/d}$, with c_1 a constant depending on k and on the density of μ. For $\alpha > \frac{1}{d}$, we thus get that $d_{\mu,m}/m^\alpha$ is decreasing with m. Therefore its minimum is reached at a value $m^* = 1$, and $\delta^2_{\mu,\alpha}$ is, in the discrete case, the average squared distance to the whole point set.

Consider now a uniform continuous measure μ on a k-subspace in d-dimensional space. At distance h from this subspace, we find that

$$d^2_{\mu,m}(h) = c_1 m^{2/k} + h^2.$$

Hence for $\alpha < \frac{1}{k}$, $d_{\mu,m}(h)/m^\alpha$ is unimodal as a function of m, and $m^*(h) = c_2 h^k$. We obtain: $\delta_{\mu,\alpha}(h) = c_3 h^{1/k-\alpha}$. Notice that this function reaches zero on the shape and grows with a vertical tangent as we move away from it: its level sets therefore accumulate way tighter around the data

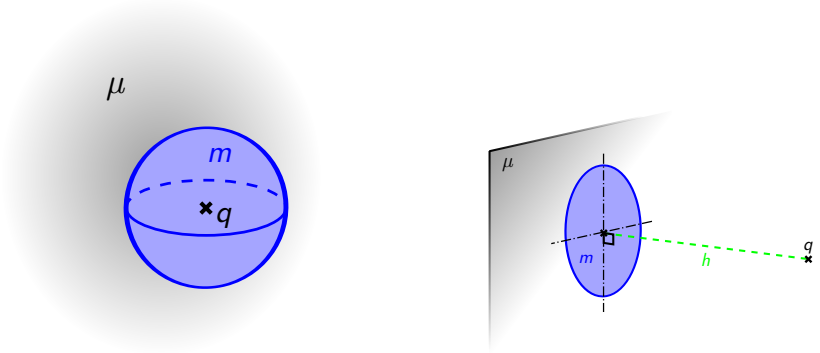

FIGURE 1. **Left: Ambient noise μ in a d-dimensional space.** A sphere centered on q contains the mass m. **Right: Uniform measure μ on a k-subspace.** A circle centered on the orthogonal projection of q on the supporting plane of μ contains the mass m.

than the non-adaptive distance function which is a smooth quadratic function that never goes to zero. We thus obtain a precise localization of the inferred shape.

Figure 2 depicts a realistic case of a noisy k-submanifold on a d-dimensional space. Depending on the value of m, it boils down to one of the two previous cases. Consider a query point q lying on the shape. At smaller scale than the noise level, the data appears as an ambient noise: for $\alpha > \frac{1}{d}$, on small values of m, $d_{\mu,m}(x)/m^\alpha$ is decreasing. As soon as the scale gets larger than the noise level, the data appears as a k-submanifold: for $\alpha < \frac{1}{k}$, $d_{\mu,m}(x)/m^\alpha$ is increasing.

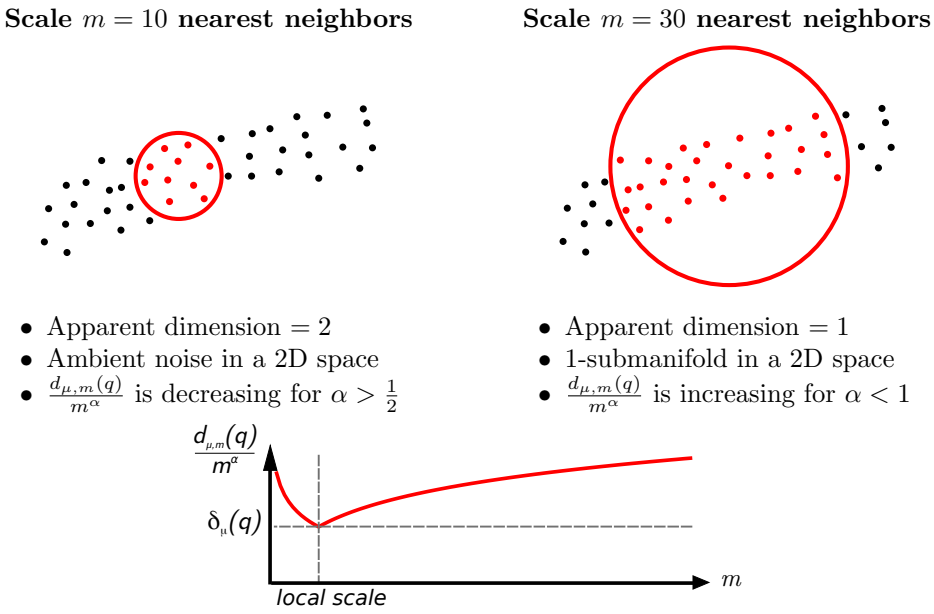

FIGURE 2. **Adaptive distance function.**

This means that under these conditions, the minimum m^* reached relates to the scale of the local noise. Consequently, the adaptive distance function provides an accurate representation of the data on noise-free areas, while sufficiently smoothing the data in poorly sampled areas. These properties are met as long as $\alpha \in]\frac{1}{d}; \frac{1}{k}[$. We thus choose $\alpha = \frac{3}{4}$ for curves in 2D and $\alpha = \frac{5}{12}$ for surfaces in 3D.

This parameter can also be set to deal with a curve in 3D: $\alpha = \frac{2}{3}$. However, this is out of scope in our context as we aim at reconstructing closed surfaces bounding a 3D solid.

To achieve correct topological inference similarly to the non-adaptive distance function, it is necessary to limit the infimum over the values of m that exceed a threshold m_0. Indeed, for a single value of m, the robust distance $d_{\mu,m}$ is $\frac{1}{\sqrt{m}}$-robust: this means that two measures μ_1 and μ_2 that are ε away in the Wasserstein 2-distance will have robust distances $d_{\mu_1,m}$ and $d_{\mu_2,m}$ at most $\frac{\varepsilon}{\sqrt{m}}$ away in the sup norm. For a single value of m, the robust distance is also 1-semiconcave. All functions in the infimum are therefore $m_0^{-\alpha-1/2}$-robust with $m_0^{-2\alpha}$-semiconcave squares. Defining this non-zero infimum m_0 for the adaptive distance function, we preserve these properties of the original non-adaptive function. In practice, we set a lower bound $K_0 = 6$ for selecting the K nearest neighbors.

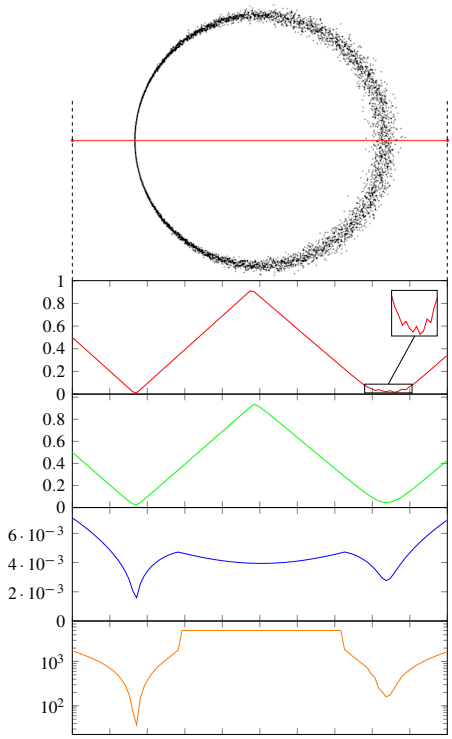

Figure 3. **Distance functions. Top:** input point set and segment selected to depict function values. **Red curve:** robust function d_μ with $K = 6$: small details are captured in noise-free area, but the function is noisy on noisy area. **Green curve:** robust function d_μ with $K = 70$: noisy areas are captured, but noise-free areas are over-smoothed and the first minimum of the function is shifted to the right. **Blue curve:** adaptive function δ_μ: all features are captured. **Orange curve:** selected value for K: notice the high dynamic of the function (log vertical scale). The flat maximum appears when the total number of points is reached.

Figure 3 compares the adaptive and non-adaptive distance functions. This new function altogether removes the need for a scale parameter and does not exhibit the defects of the globally-scaled and non-adaptive function. A curve also depicts the local scale as value of K where the minimum is reached.

The reconstruction algorithm consists in computing an implicit function whose 0-isolevel defines the shape. It comprises two main steps: (i) Computing the adaptive distance function, and (ii) Signing it by estimating the sign of a signed version of this distance function on a set of discrete locations, and propagating the sign guesses using the adaptive distance function.

Unsigned Distance. We represent the adaptive distance function by linear interpolation on the triangles of an isotropic triangulation. The latter is obtained through adaptive Delaunay refinement such that the interpolated and real values are ε away from each other (see Figure 4). For each vertex

of the triangulation computing the adaptive distance function amounts to search for a minimum over all possible K nearest neighbors, leading to a major scalability issue. Instead of performing an exhaustive search, we rely on a k-d tree structure for neighbor search, combined to a hierarchical clustering of the input point set [10].

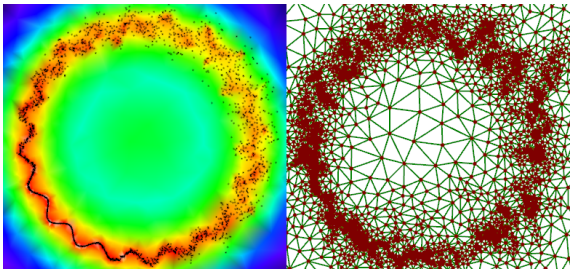

FIGURE 4. **Delaunay refinement.** Left: input point set and distance function. Right: output triangulation.

Signing. We first guess the sign of the output implicit function on a discrete set of points. The latter are selected as the corners of a regular grid that covers the domain of the input set (defined as a loose bounding box). Edges are randomly picked on this grid and each of them is assigned a sign estimate $\varepsilon_{i,j}$ that is -1 or $+1$, depending if the two end nodes i and j are estimated to be on the same side or on opposite sides of the shape. Then, by minimizing the following energy: $E_G(f) = \sum_{(i,j)\in G}(f_i + \varepsilon_{i,j} f_j)^2$, a sign f_i is estimated for all the nodes i. A confidence is derived for each node as the ratio of sign hypothesis on edges that are matched by the output signs of the nodes. Figure 5 illustrates the sign guess pipeline.

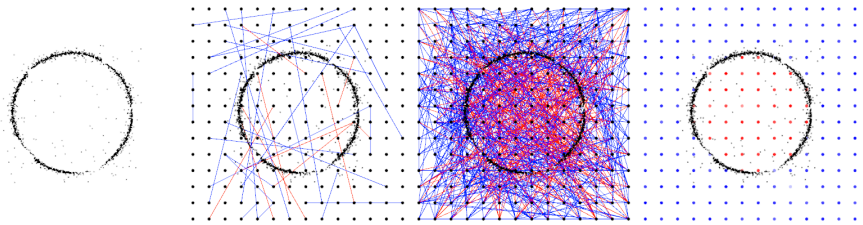

FIGURE 5. **Random graph.** From left to right: input point set; edges of the graph (only 1% of edges are shown for clarity, with blue for similar signs and red for different signs); 20% of the graph edges shown; signed function at graph nodes after linear solve (red for inside, blue for outside).

Given the set of most confident sign guesses and the adaptive unsigned distance function, the output signed implicit function is computed using a method inspired by the random walker approach used for image segmentation [11]. Figure 6 illustrates resilience to gradually variable noise: the reconstructed surface smoothly approximates the inferred shape on noisy area while providing high accuracy on noise-free area. We compare to the Poisson reconstruction approach which relies upon a single scale parameter. Both algorithms are timed on GNU/Linux with a 4-core 2.4 GHz *Intel Core i7* processor with 8 GB of RAM.

Figure 7 depicts our algorithm at work on a point set generated by photogrammetry. To evaluate resilience to variable noise we add a synthetic noise on the top half part of the point set.

3. Piecewise Smooth Reconstruction

For piecewise smooth shapes with boundaries we reformulated 2D shape reconstruction and simplification in a preliminary work [6] as a transportation problem between measures (*i.e.*, mass

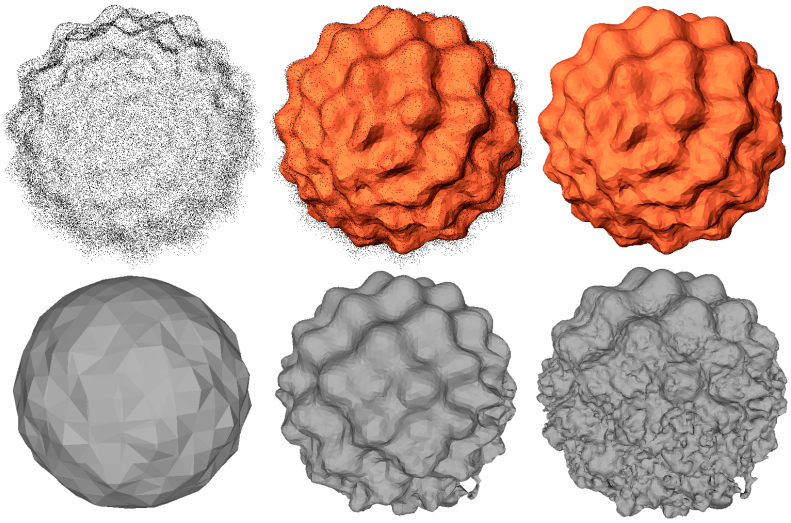

Figure 6. **Gradually variable noise (generated).** Top: raw point set, where noise increases linearly from top to bottom; point set & our reconstruction; our reconstruction only (running time: 82s). Bottom: Poisson reconstruction with a uniform octree depth of 4, 6 and 8 (running times: 1, 10 and 50s respectively).

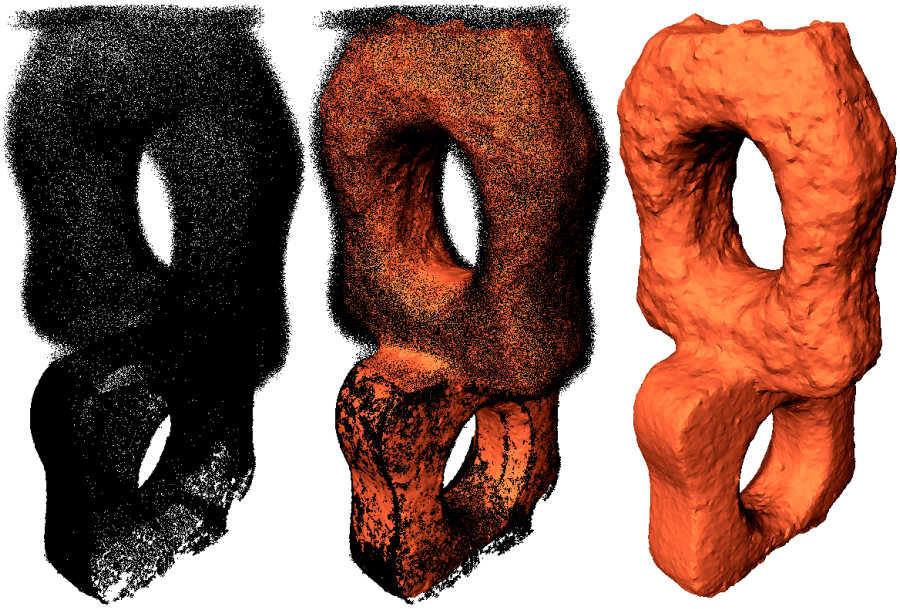

Figure 7. **Two levels of noise**. Left: raw point set with additional noise on the top half part. Middle: point set & reconstruction. Right: reconstruction only (running time: 242s).

distributions), where the input point samples are considered as Dirac measures and the reconstructed shape is seen as the support of a continuous measure defined on the vertices and edges of a 2D triangulation. Our formulation significantly differs from the common way to state the optimal transportation problem in the sense that we do not know the target measure but instead need to solve for it. We restrict the target measure to be defined as the sum of piecewise uniform measures on the simplices of a 2D triangulation. When the transport plan is restricted to transport each input point sample to the nearest edge of the triangulation, the optimal transport cost based on the Wasserstein-2 distance is computed in closed form. The final triangulation is obtained through greedy decimation of an initial dense Delaunay triangulation constructed with the input

point samples, where the decimation operators are ordered so as to minimally increase the total transport cost. This approach both reconstructs and generates a simplified shape, and brings forth a unified treatment of noise, outliers and boundaries (Figure 8).

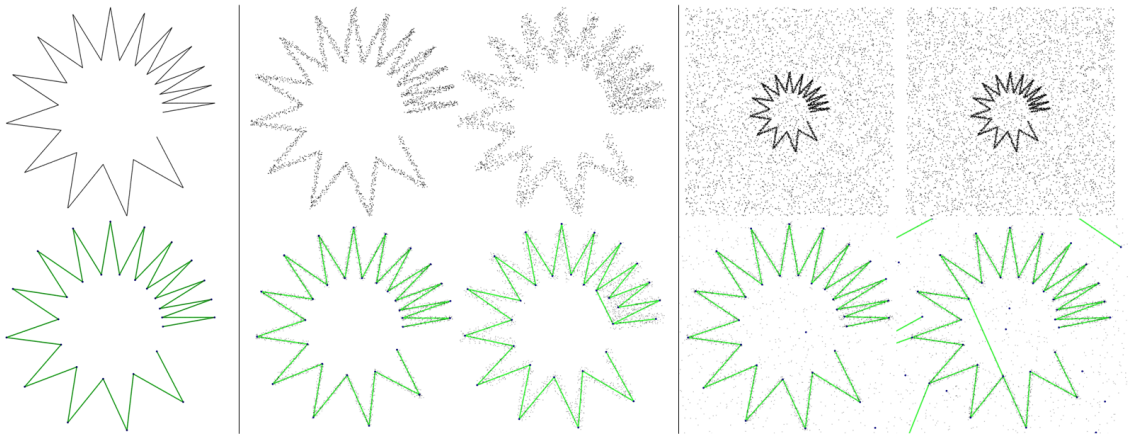

FIGURE 8. **Robust 2D shape reconstruction and simplification.** The input shape (3K points) has sharp corners subtending small angles as well as boundaries. The reconstruction is perfect for a noise-free input (left); as noise is added (middle, 2% and 2.5% of bounding box), the output degrades gracefully, still capturing most of the sharp angles; after adding 4K or 4.5K outliers and 2% of noise (right), the reconstruction remains satisfactory, although artifacts start appearing in this regime.

Without restricting the transport plan such that each sample point can be transported to an arbitrary edge of the triangulation there is no closed form anymore as the structure of the transport plan becomes a variable of the problem. As first direction we performed a pointwise discretization of each edge of the triangulation before resorting to a dense linear program to determine the point-to-point optimal transport plan and associated cost. The latter approach is very computer-intensive but exhibits even better resilience to noise and outliers.

The linear programming approach described above applies to noise and outlier-robust reconstruction of surfaces with sharp features and boundaries. However, and even when using the restricted transport plan as mentioned above, there is no closed form when dealing with the facets of a triangulated surface. Computing the optimal transport cost and plan through pointwise discretization and linear programming is thus substantially more computer-intensive than for 2D shapes.

For surfaces we formulate the reconstruction problem as a transportation problem between measures (i.e., mass distributions), where the input point samples are considered as Dirac measures and the reconstructed shape is seen as the support of a piecewise uniform measure over the simplices (vertices, edges, facets) of a surface simplicial complex [8]. Using three different types of simplices provides us with a means to deduce the local dimension from the optimal transport plan found by the solver.

To obtain high robustness to noise and outliers we formulate the problem with a general transport plan where each input sample point can be split into sub-masses, each transported to different locations on the complex. We thus use a discretized formulation of the optimal transport problem, where we approximate the optimal transport cost between the input point set $\mathcal{S}$ and the simplicial complex $\mathcal{C}$ using quadrature intervals, which we call hereafter *bins*. To this end, we partition vertices, edges, and facets of $\mathcal{C}$ into a set of bins $\mathcal{B}$ and evaluate the optimal cost between $\mathcal{S}$ and $\mathcal{B}$ as the sum of squared distances between the points in $\mathcal{S}$ and the centroid of the bins in $\mathcal{B}$. Bins on facets are constructed as the bounded Voronoi cells of a centroidal Voronoi tessellation (see inset). In order to accommodate the non-uniform distribution of bins, we assign a *capacity* for

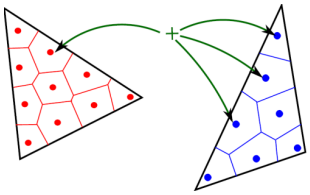

each bin in $\mathcal{B}$ (i.e., the total amount of mass that a bin can receive).
While we set vertex bins to unit capacity, edge bins and facet bins are
respectively assigned capacities proportional to the lengths and areas of the Voronoi cells.

We use a linear programming formulation to compute the optimal transport cost between the input point set $\mathcal{S}$ and the bin set $\mathcal{B}$. In the following, we denote the simplices of $\mathcal{C}$ as $\{\sigma_j\}_{j=1\cdots L}$ and the bins in $\mathcal{B}$ as $\{b_j\}_{j=1\cdots M}$, where L and M are the number of simplices and bins respectively. We also define $s(j)$ to be the index of the simplex containing the bin b_j (i.e., $b_j \in \sigma_{s(j)}$). The capacity c_j of bin b_j is defined as the ratio between the bin's area and the area of its containing simplex. Finally, we denote m_{ij} as the amount of mass transported from point $p_i \in S$ to the centroid of bin b_j.

With these definitions, we can now refer to a *transport plan* between $\mathcal{S}$ and $\mathcal{B}$ as a set of $N \times M$ variables m_{ij} such that:

$$\forall ij : \; m_{ij} \geq 0, \tag{3.1}$$

$$\forall i : \; \sum_j m_{ij} = m_i, \tag{3.2}$$

$$\forall j_1, j_2 \text{ s.t. } s(j_1) = s(j_2) : \; \frac{1}{c_{j_1}} \sum_i m_{ij_1} = \frac{1}{c_{j_2}} \sum_i m_{ij_2}, \tag{3.3}$$

where Equation 3.2 ensures that the entire measure of a point gets transported onto simplices, and Equation 3.3 ensures a uniform measure over each simplex of $\mathcal{C}$. An *optimal transport plan* is then defined as a transport plan π that minimizes the associated transport cost

$$cost(\pi) = \sum_{ij} m_{ij} \|p_i - b_j\|^2.$$

Finding a transport plan minimizing the transport cost results in a linear program with respect to the m_{ij}, with equality (Eq. 3.2 and 3.3) as well as inequality constraints (Eq. 3.1). In order to enforce the uniformity constraint (Eq. 3.3), we also introduce L additional variables l_i (one per simplex σ_i) indicating the target measure density of the corresponding simplex. The final formulation is thus:

$$\text{Minimize} \quad \textstyle\sum_{ij} m_{ij} \|p_i - b_j\|^2$$

w.r.t. the variables m_{ij} and l_j, and subject to:

$$\begin{cases} \forall i : \displaystyle\sum_j m_{ij} = m_i \\ \forall j : \displaystyle\sum_i m_{ij} = c_j \cdot l_{s(j)} \\ \forall i,\ j : m_{ij} \geq 0,\ l_j \geq 0 \end{cases}$$

Our reconstruction algorithm proceeds by iterative decimation – through half edge collapse operators – of a 2-simplicial complex initialized as the facets of the 3D Delaunay triangulation constructed from a subset of the input points (Figure 9). We also couple our decimation with an optimization procedure in order to relocate the vertices in the reconstructed simplicial complex. This optimization procedure further minimizes the transport cost through alternating vertex relocation (with a fixed transport plan) and re-computation of the optimal transport plan. The edge collapse operators are our means to generate a simplicial complex with anisotropic triangle facets where relevant from the approximation point of view.

4. **Conclusion**

We described two recent contributions for noise and outlier robust shape reconstruction, both derived from computing and minimizing distances between measures through optimal transportation.

For smooth, closed shapes we compute and sign a noise-adaptive distance function before extracting one its isolevel as final reconstruction. For piecewise smooth shapes with boundaries we proceed by iterative, feature-preserving simplification of a simplicial complex constructed from the input point set. To achieve noise and outlier robustness, an error metric driving the simplification

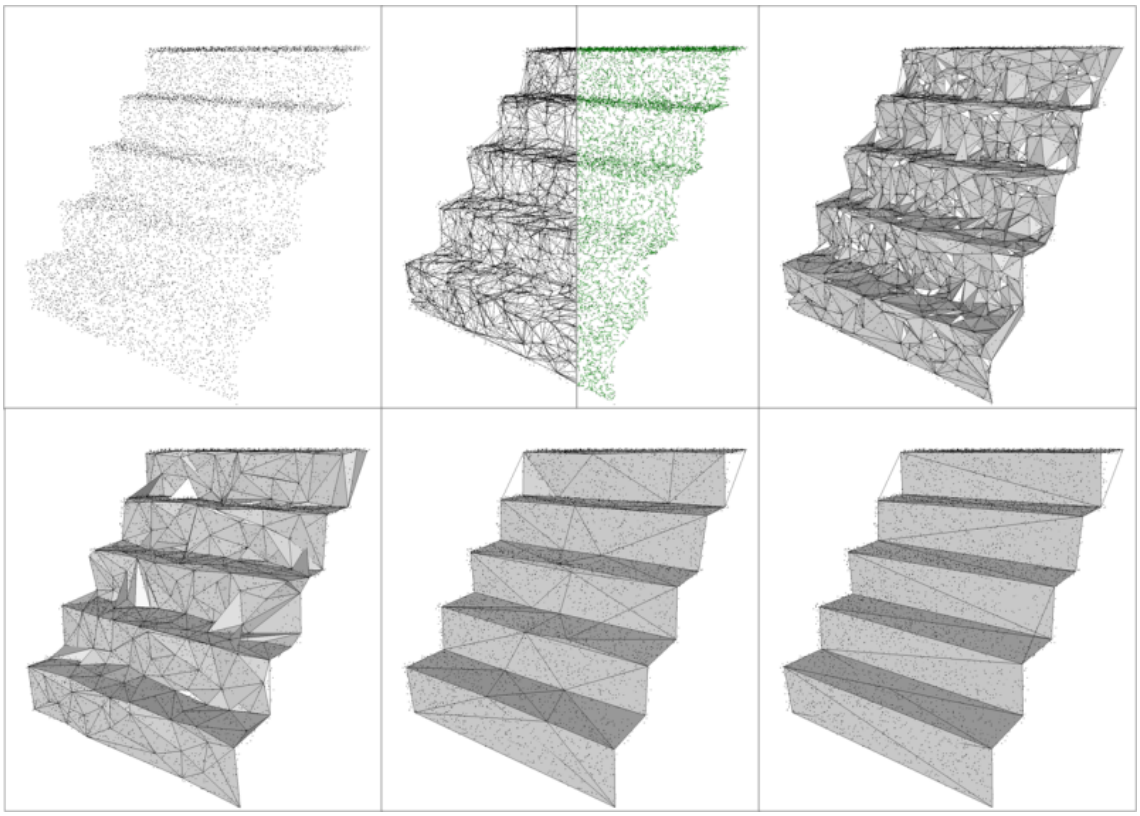

FIGURE 9. **Robust surface reconstruction and simplification.** Top: Initial point set; Filtered 3D Delaunay triangulation of a random subset containing 10% of the input points and initial transport plan assigning point samples to discretization points (green arrows); and first few decimation step. Bottom: Reconstruction with 100, 50, and 14 vertices, respectively.

is derived in terms of optimal transport between the input point set and the reconstructed mesh, both seen as mass distributions. Even when restricting the transport plan to transport input samples to local neighborhoods, our solution based on linear programming has a high computational cost: we need to gain 4 orders of magnitude to obtain a practical algorithm. In the future we plan to investigate how to compute an estimate of the optimal transport cost. We also plan to perform a statistical analysis of the optimal transport plan per simplex in order to devise a more parsimonious shape refinement algorithm. Intuitively, the transport cost will be used to decide where to refine the shape, while the transport plan analysis translates into how to refine, namely into the type and parameters of a local anisotropic refinement operator.

Bibliography

[1] Haim Avron, Andrei Sharf, Chen Greif, and Daniel Cohen-Or. ℓ_1-sparse reconstruction of sharp point set surfaces. *ACM Trans. on Graphics*, 29(5):1–12, 2010.

[2] Haim Avron, Andrei Sharf, Chen Greif, and Daniel Cohen-Or. L1-sparse reconstruction of sharp point set surfaces. *ACM Transactions on Graphics*, 29:135:1–135:12, November 2010.

[3] Nicolas Bonneel, Michiel van de Panne, Sylvain Paris, and Wolfgang Heidrich. Displacement interpolation using lagrangian mass transport. *ACM Transactions on Graphics (SIGGRAPH Asia Proceedings)*, 2011.

[4] Frédéric Cazals and Joachim Giesen. Delaunay triangulation based surface reconstruction. In J.D. Boissonnat and M. Teillaud, editors, *Effective Computational Geometry for Curves and Surfaces*, pages 231–276. Springer-Verlag, Math. and Visualization, 2006.

[5] Frédéric Chazal, David Cohen-Steiner, and Quentin Mérigot. Geometric inference for probability measures. *Journal on Foundations of Computational Mathematics*, 11:733–751, 2011.

[6] Fernando de Goes, David Cohen-Steiner, Pierre Alliez, and Mathieu Desbrun. An Optimal Transport Approach to Robust Reconstruction and Simplification of 2D Shapes. *Computer Graphics Forum*, 30(5):1593–1602, 2011. Special issue for EUROGRAPHICS Symposium on Geometry Processing.

[7] Tamal K. Dey. *Curve and Surface Reconstruction: Algorithms with Mathematical Analysis*. Cambridge Monographs on Applied and Computational Mathematics, 2006.

[8] Julie Digne, David Cohen-Steiner, Pierre Alliez, Fernando Goes, and Mathieu Desbrun. Feature-preserving surface reconstruction and simplification from defect-laden point sets. *Journal of Mathematical Imaging and Vision*, pages 1–14, 2013.

[9] S. Fleishman, D. Cohen-Or, and C.T. Silva. Robust moving least-squares fitting with sharp features. In *ACM SIGGRAPH 2005 Papers*, page 552, 2005.

[10] Simon Giraudot, David Cohen-Steiner, and Pierre Alliez. Noise-Adaptive Shape Reconstruction from Raw Point Sets. *Computer Graphics Forum*, 32(5):229–238, 2013.

[11] Leo Grady. Random walks for image segmentation. *Pattern Analysis and Machine Intelligence, IEEE Transactions on*, 28(11):1768–1783, 2006.

[12] Michael Kazhdan, M. Bolitho, and Hugues Hoppe. Poisson Surface Reconstruction. In *Symposium on Geometry Processing*, pages 61–70, 2006.

[13] Ravikrishna Kolluri, Jonathan Shewchuk, and James O'Brien. Spectral surface reconstruction from noisy point clouds. In *Proceedings of EUROGRAPHICS Symposium on Geometry Processing*, pages 11–21, 2004.

[14] Yaron Lipman and Ingrid Daubechies. Surface comparison with mass transportation. ArXiv preprint 0912.3488, 2010.

[15] Patrick Mullen, Fernando De Goes, Mathieu Desbrun, David Cohen-Steiner, and Pierre Alliez. Signing the unsigned: Robust surface reconstruction from raw pointsets. *Computer Graphics Forum*, 29(5):1733–1741, 2010. Proceedings of EUROGRAPHICS Symposium on Geometry Processing.

[16] Yuqing Song. Boundary fitting for 2D curve reconstruction. *The Visual Computer*, 26:187–204, 2010.

[17] S. Sotoodeh. Outlier detection in laser scanner point clouds. *International Archives of Photogrammetry, Remote Sensing and Spatial Information Sciences*, 36(5):297–302, 2006.

[18] C. Villani. *Topics in Optimal Transportation*. American Mathematical Society, 2010.

Pierre Alliez
Inria Sophia Antipolis - Mediterranée
2004 route des Lucioles
06902 Sophia Antipolis
FRANCE
pierre.alliez@inria.fr

Simon Giraudot
Inria Sophia Antipolis - Mediterranée
2004 route des Lucioles
06902 Sophia Antipolis
FRANCE
simon.giraudot@inria.fr

David Cohen-Steiner
Inria Sophia Antipolis - Mediterranée
2004 route des Lucioles
06902 Sophia Antipolis
FRANCE
david.cohen-steiner@inria.fr